

Near-Infrared Coloring via a Contrast-Preserving Mapping Model

Chang-Hwan Son and Xiao-Ping Zhang, *Senior Member IEEE*

Abstract— Near-infrared gray images captured along with corresponding visible color images have recently proven useful for image restoration and classification. This paper introduces a new coloring method to add colors to near-infrared gray images based on a contrast-preserving mapping model. A naive coloring method directly adds the colors from the visible color image to the near-infrared gray image. However, this method results in an unrealistic image because of the discrepancies in the brightness and image structure between the captured near-infrared gray image and the visible color image. To solve the discrepancy problem, first we present a new contrast-preserving mapping model to create a new near-infrared gray image with a similar appearance in the luminance plane to the visible color image, while preserving the contrast and details of the captured near-infrared gray image. Then we develop a method to derive realistic colors that can be added to the newly created near-infrared gray image based on the proposed contrast-preserving mapping model. Experimental results show that the proposed new method not only preserves the local contrast and details of the captured near-infrared gray image, but also transfers the realistic colors from the visible color image to the newly created near-infrared gray image. It is also shown that the proposed near-infrared coloring can be used effectively for noise and haze removal, as well as local contrast enhancement.

Index Terms— Coloring, color transfer, contrast enhancement, denoising, dehazing, image fusion, near-infrared imaging

I. INTRODUCTION

Near-infrared imaging was developed to consecutively capture near-infrared gray images and visible color images [1]. In general, a hot mirror is used to prevent the near-infrared part of the electromagnetic spectrum, ranging from 750 to 1400 nm, from reaching sensitive CMOS sensors and contaminating the visible color images. However, if the hot mirror is replaced with a piece of clear glass and a pair of lens-mounted filters to block or pass the near-infrared region, a visible color image and its corresponding near-infrared gray image can be captured. This pair of images often has different pixel information for the same scene. The resulting redundant information can be helpful in certain tasks, including image denoising [2], deblurring [3], dehazing [4], and classification [5].

This work was supported by the National Research Foundation of Korea (2017R1D1A3B03030853), the Natural Sciences and Engineering Research Council of Canada (NSERC) under Grant RGPIN239031.

C.-H. Son is with the Department of Software Convergence Engineering, Kunsan National University, Gunsan-si, 54150, South Korea (E-mail: changhwan76.son@gmail.com.)

X.-P. Zhang is with the Department of Electrical and Computer Engineering, Ryerson University, ON M5B2K3 Canada (E-mail: xzhang@ryerson.ca).

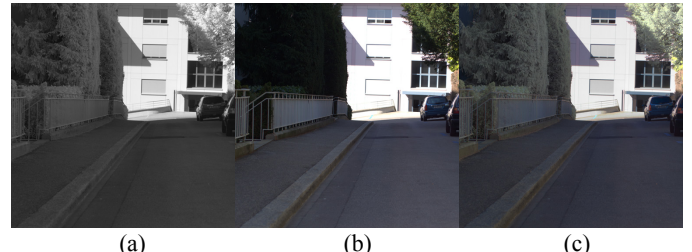


Fig. 1. (a) captured near-infrared gray image, (b) captured visible color image, and (c) colored near-infrared image.

A. Motivation

The objective of this paper is to provide a new way to color a near-infrared gray image. This is ostensibly easy to accomplish because visible color images are available. It is tempting to use a naive coloring method that merely combines the chrominance planes from the visible color image with the near-infrared gray image in an opponent color space. However, discrepancies can emerge between the near-infrared gray image and the visible color image. In other words, the brightness and image structure of near-infrared gray images can differ from those of the visible color images. An example is provided in Fig. 1. In Fig. 1(a), the near-infrared gray image shows the leaves on the tree and the lines on the wall. However, they are absent in the visible color image in Fig. 1(b). This is caused by the low dynamic range of the camera that leads to pixel saturation in the dark and bright regions. Therefore, a naive coloring method to directly add colors from the visible color image to the near-infrared gray image results in unnatural colors, as shown in Fig. 1(c). In particular, the tree color in the colored near-infrared image does not look natural, in contrast to the natural tree color in the visible color image. In this paper, we focus on developing a method to solve this discrepancy so that the natural colors from the visible color image can be transferred to a near-infrared gray image without any loss of detail and contrast.

B. Contributions

- A new method for transferring the colors from a visible color image to a near-infrared gray image is presented. We first model a contrast-preserving linear mapping between the two images. This mapping model is used to generate a new near-infrared gray image and correct the chrominance distribution of the visible color image, thereby transferring realistic colors to the newly created near-infrared gray image. The proposed mapping model can resolve the discrepancy between the near-infrared gray image and visible color image.

- A detail layer transfer method based on the detail difference constraint is introduced to enhance the detail layer of the newly created near-infrared gray image. The detail difference constraint forces the gradients of the detail layer of the newly created near-infrared gray image to be closer to those of the captured near-infrared gray image. By adopting this detail difference constraint, detail description and the amount of visual information can be improved.
- Conventional methods [1–4] focus on fusing images to increase visual information or edge representation. However, the proposed method is concerned with transferring the colors from the visible color image to the near-infrared gray image without any loss of detail and contrast. The differences between the conventional and proposed methods are discussed in this paper. The experimental results confirm that the proposed method is more effective at expressing local color contrast and detail than conventional methods.
- In dim lighting conditions, captured visible color images may contain significant noise. In this case, the question arises as to whether the proposed method is effective on the captured image pair of a noisy visible color image and the near-infrared gray image. The experimental results show that the proposed approach used for the near-infrared coloring can also be applied to image pairs captured under dim lighting conditions. The differences between the proposed near-infrared denoising and conventional image-pair-based fusion [2,3,6,7,8,9,10] are discussed. It is shown that the proposed near-infrared coloring method can also be used for haze removal and local contrast enhancement.
- Part of work in this paper was presented in our conference paper [11]. Compared to [11], it is shown in this paper how the proposed near-infrared coloring with a little modification can be used for noise removal. Moreover, in the experimental results, it is shown that the proposed method can also be applied to other applications: haze removal and local contrast enhancement. Furthermore, quantitative evaluation is added and more conventional methods are compared.

C. Notation

In this paper, bold lowercase is used to indicate column vectors. For example, \mathbf{x}^v and \mathbf{x}^{nir} indicate the column vectors that contain the pixel values of the captured visible color image and near-infrared gray image, respectively. The superscripts are used to differentiate between the two images. If the captured images are not grayscale, round brackets are used to indicate the luminance and chrominance planes such as $\mathbf{x}^{v(l)}$ and $\mathbf{x}^{v(e)}$. In order to denote the pixel location, the subscript i is used like \mathbf{x}_i^v . $\|\cdot\|$ indicates the l_2 -norm and $|\cdot|$ denotes an absolute value. N is a total number of pixels.

II. RELATED WORKS

A. Regularization Approach

The discrepancy problem appears when a naive coloring

method combining the chrominance planes of the visible color image with the near-infrared gray image is used. One solution is to adopt a regularization approach [3,6,7] that has been widely used for image-pair-based restoration. The regularization term can be modeled as follows:

$$\min_{\mathbf{x}} \left\{ \mu_g \cdot \left\| \mathbf{x} - \mathbf{x}^{v(l)} \right\|^2 + \sum_{j=1}^2 \sum_{i=1}^N \left| (\mathbf{x} \otimes f^j)_i - (\mathbf{x}^{nir} \otimes f^j)_i \right|^{\gamma} \right\} \quad (1)$$

where $\mathbf{x}^{v(l)}$ and \mathbf{x}^{nir} represent the luminance plane for the visible color image and the near-infrared gray image, respectively, and f denotes the horizontal or vertical derivative filter. In (1), the first term, i.e., the data-fidelity term, indicates that the unknown luminance image to be estimated is similar to the luminance plane for the visible color image. To improve the edge representation, a regularization term is provided by the second term in (1). This constraint forces the edges from the unknown luminance plane to be close to those in the near-infrared gray image. In (1), γ is a constant value that controls the sparsity [8]. In general, the value of γ is less than one. Given an estimated luminance plane, its colors can be taken directly from the visible color image. In other words, the estimated luminance plane can be combined with the chrominance planes from the visible color image.

B. Multiresolution Approach

Another approach is to apply multiresolution techniques [1,9,10] widely used for image fusion. The wavelet transform is a well-known multiresolution representation. The luminance plane for the visible color image can be combined in the multiresolution subspace with the near-infrared gray image as follows:

$$\Theta(\mathbf{x}) = \begin{cases} \alpha_l \Theta(\mathbf{x}^{v(l)}) + (1 - \alpha_l) \Theta(\mathbf{x}^{nir}) & \text{for LL subband} \\ \text{MAX}(\Theta(\mathbf{x}^{v(l)}), \Theta(\mathbf{x}^{nir})) & \text{for other subbands} \end{cases} \quad (2)$$

where $\Theta(\mathbf{x}^{v(l)})$ and $\Theta(\mathbf{x}^{nir})$ represent the wavelet coefficients of the luminance plane for the visible color image and the near-infrared gray image, respectively, and MAX denotes the function that returns the largest value of a set of values. The above equation shows that the wavelet coefficients of the luminance plane for the visible color image are linearly mixed with those of the near-infrared gray image for the lowest frequency subband. For other subbands, the larger wavelet coefficient between $\Theta(\mathbf{x}^{v(l)})$ and $\Theta(\mathbf{x}^{nir})$ is selected to increase the details of the fused image. Given the created luminance plane, according to (2), its colors can be taken directly from the visible color image.

C. Statistical Approach

In [12], mean and variance, the representative statistics of natural images, are used to transfer the color appearance of a reference image to that of a target image. This approach can be adopted to solve the near-infrared coloring problem. The local mean and variance of the luminance plane for the visible color image can be changed according to the local mean and variance

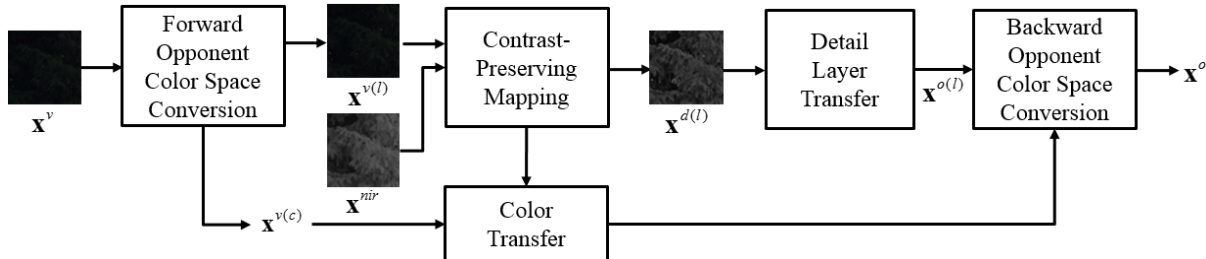


Fig. 2. Block-diagram of proposed method.

of the near-infrared gray image as follows:

$$\mathbf{x}_i^{o(l)} = \mu_i^{nir} + (\mathbf{x}_i^{v(l)} - \mu_i^{v(l)}) \cdot \frac{\sigma_i^{nir}}{\sigma_i^{v(l)}} \quad \text{and} \quad \mathbf{x}_i^{o(c)} = \mathbf{x}_i^{v(c)} \cdot \frac{\sigma_i^{nir}}{\sigma_i^{v(l)}} \quad (3)$$

where μ_i and σ_i denote the mean and variance of the local patch centered at the i th pixel location, respectively, and $\mathbf{x}_i^{o(l)}$ and $\mathbf{x}_i^{o(c)}$ represent the i th pixel values of the luminance and chrominance planes of the colorized image, respectively. The above equation tells us that the luminance plane of the visible color image $\mathbf{x}_i^{v(l)}$ can be scaled according to the variance ratio $\sigma_i^{nir}/\sigma_i^{v(l)}$. In addition, the new chrominance planes $\mathbf{x}_i^{o(c)}$ can also be created by scaling the chrominance planes $\mathbf{x}_i^{v(c)}$ of the visible color image by the variance ratio.

III. PROPOSED NEAR-INFRARED COLORING

Figure 2 shows a block-diagram of the proposed method. First, the visible color image \mathbf{x}^v is separated into the luminance and chrominance planes $\mathbf{x}^{v(l)}$ and $\mathbf{x}^{v(c)}$ through a forward opponent color space conversion [12]. Then the proposed contrast-preserving mapping is applied to the image pair consisting of the near-infrared gray image \mathbf{x}^{nir} and the luminance plane of the visible color image $\mathbf{x}^{v(l)}$. The details and visual information of the newly created luminance plane $\mathbf{x}^{d(l)}$ via the contrast-preserving mapping are further enhanced by the detail layer transfer. The relation between \mathbf{x}^{nir} and $\mathbf{x}^{v(l)}$ established via the contrast-preserving mapping is used for the color transfer, which changes the color distribution of the chrominance plane $\mathbf{x}^{v(c)}$. Next, the detail-enhanced version $\mathbf{x}^{o(l)}$ of the newly created luminance plane is combined with the modified chrominance plane. Finally, the colored output image \mathbf{x}^o is obtained via the backward opponent color space conversion.

A. Proposed Approach

The central idea of the proposed near-infrared coloring method is the contrast-preserving mapping model. As shown in Fig. 1, the discrepancy problem results in unnatural colors. To handle this issue, a contrast-preserving mapping model is proposed. The first role of this model is to create a new near-infrared gray image. As shown in Fig. 2, the newly created near-infrared gray image $\mathbf{x}^{d(l)}$ can preserve the detail and local contrast of the near-infrared gray image \mathbf{x}^{nir} . The input visible and near-infrared patches, as shown in Fig. 2, are extracted from the tree region of Fig. 1. Note that the newly created near-infrared gray

image $\mathbf{x}^{d(l)}$ is different from the captured near-infrared gray image \mathbf{x}^{nir} .

The second role of the model is to determine the mapping relation between the near-infrared gray image \mathbf{x}^{nir} and the visible color image $\mathbf{x}^{v(l)}$. A critical point of the proposed coloring method is that it adds unknown colors to the newly created near-infrared gray image $\mathbf{x}^{d(l)}$, not the captured near-infrared gray image \mathbf{x}^{nir} . To estimate the unknown colors of the newly created near-infrared gray image, the mapping relation obtained using the contrast-preserving mapping is utilized. That is, the mapping relation provides a new color transfer model to predict the unknown colors from the chrominance images $\mathbf{x}^{v(c)}$ of the visible color image.

B. Contrast-Preserving Linear Mapping

To transfer the colors from the visible color image to the near-infrared gray image without any loss of detail, a contrast-preserving mapping is needed. The objective of the proposed contrast-preserving mapping is to find the relation between the luminance plane for the visible color image and near-infrared gray image. Based on this mapping relation, another near-infrared gray image is generated that preserves the local contrast. Furthermore, the color corresponding to the newly created near-infrared gray image can be estimated. The proposed contrast-preserving mapping model is formulated as follows:

$$\min_{\mathbf{a}} \left\| \mathbf{W}_i^{1/2} (\mathbf{p}_i - \mathbf{Q}_i \mathbf{a}_i) \right\|^2 + \mu_c \left\| \mathbf{a}_i - \mathbf{a}_i^0 \right\|^2 \quad (4)$$

where \mathbf{p}_i and \mathbf{Q}_i contain the pixel values of the extracted patches from the luminance plane of the visible color image and the near-infrared image at the i th pixel location, respectively. A decorrelated color space [12] is used to generate the luminance plane. Other opponent color spaces, e.g., CIELAB or YCbCr [1], could be considered. Assuming that the extracted patch has an odd size $m \times m$, \mathbf{p}_i and \mathbf{Q}_i can be defined as follows:

$$\mathbf{p}_i = \mathbf{R}_i \mathbf{x}^{v(l)} = \left[\mathbf{x}_{i-m/2}^{v(l)}, \mathbf{x}_{i-m/2+1}^{v(l)}, \dots, \mathbf{x}_i^{v(l)}, \dots, \mathbf{x}_{i+m/2-1}^{v(l)}, \mathbf{x}_{i+m/2}^{v(l)} \right]^T \quad (5)$$

$$\mathbf{Q}_i = [\mathbf{R}_i \mathbf{x}^{nir} \mathbf{1}] = \left[\mathbf{x}_{i-m/2}^{nir}, \mathbf{x}_{i-m/2+1}^{nir}, \dots, \mathbf{x}_i^{nir}, \dots, \mathbf{x}_{i+m/2-1}^{nir}, \mathbf{x}_{i+m/2}^{nir} \right]^T \mathbf{1} \quad (6)$$

where \mathbf{R}_i is a matrix that extracts the patch at the i th pixel location from an image [13] and T denotes the transpose

operator. In (6), $\mathbf{1}$ indicates the column vector filled with one. If $\mathbf{x}^{v(l)}$ and \mathbf{x}^{nir} are image vectors that are $N \times 1$ in size, the matrix \mathbf{R}_i has dimensions $m^2 \times N$. In (4), \mathbf{W} is a diagonal matrix consisting of weights that are inversely proportional to the distance between the center pixel location i and its neighboring pixel location. Vector $\mathbf{a}_i^T = [\alpha_{i,1} \ \alpha_{i,2}]$ contains two elements indicating the slope and bias, respectively. Therefore, the data fidelity term $\|\mathbf{W}_i^{1/2}(\mathbf{p}_i - \mathbf{Q}_i \mathbf{a}_i)\|^2$ from (4) can be regarded as a linear mapping. The near-infrared luminance patch $\mathbf{R}_i \mathbf{x}^{nir}$ is mapped to the visible luminance patch $\mathbf{R}_i \mathbf{x}^{v(l)}$ without any constraints. Adding a local contrast-preserving regularization term $\|\mathbf{a}_i - \mathbf{a}_i^0\|$ prevents this. Under regularization, \mathbf{a}_i^0 is given as follows:

$$\mathbf{a}_i^0 = \omega_1 \left[\mathbf{x}_i^{nir} / \text{avg}(\mathbf{R}_i \mathbf{x}^{nir}) \ 0 \right]^T + \omega_2 \left[\mathbf{x}_i^{v(l)} / \text{avg}(\mathbf{R}_i \mathbf{x}^{v(l)}) \ 0 \right]^T \quad (7)$$

where avg denotes the averaging function. The above equation indicates that the center-pixel values from the extracted near-infrared and visible-luminance patches are divided by their respective average values, and then combined linearly with weights set by the variance ratio between the two patches. The ratio of the center-pixel's brightness to the background brightness, as shown in (7), can be used as the local contrast measure [14, 15]. The slope of $\alpha_{i,1}$ corresponds to the local contrast in an image. The slope \mathbf{a}_i for the estimated linear mapping $\mathbf{Q}_i \mathbf{a}_i$ preserves local contrast \mathbf{a}_i^0 for both the near-infrared and visible luminance patches. The closed-form solution to (4) is given as follows:

$$\mathbf{a}_i = (\mathbf{Q}_i^T \mathbf{W}_i \mathbf{Q}_i + \mu_c \mathbf{I})^{-1} (\mathbf{Q}_i^T \mathbf{W}_i \mathbf{p}_i + \mu_c \mathbf{a}_i^0) \quad (8)$$

where \mathbf{I} is the identity matrix. Given the estimated \mathbf{a}_i , the pixel value of the newly created near-infrared luminance image at the i th pixel location can be obtained as follows:

$$\mathbf{x}_i^{d(l)} = \mathbf{x}_i^{nir} \alpha_{i,1} + \alpha_{i,2} \quad (9)$$

where $\mathbf{x}_i^{d(l)}$ is the newly created near-infrared luminance image with the contrast-preserving mapping. Here, \mathbf{a}_i is the linear-mapping relation between the luminance images.

C. Validity of Linear Mapping Model

In (4), the relation between the near-infrared luminance image and luminance plane of the visible color image is modeled by a linear mapping function. To verify this assumption, the linear mapping model was evaluated with respect to mean square error (MSE). The image pairs of the visible color and near-infrared gray images, as shown in Figs. 1, 5, and 6, are tested. The MSE is defined as $\|\mathbf{x}^{v(l)} - \mathbf{x}^{d(l)}\|^2 / N$. The pixel range of the tested images is scaled to $[0-1]$ and the value of μ_c

TABLE I
MSE EVALUATION

Test Images	Figs. 1(a) and (b)	Figs. 5(a) and (b)	Figs. 6(a) and (b)
MSE	2.1×10^{-5}	4.1×10^{-5}	6.5×10^{-5}

in (4) is set to zero. Table I shows that the calculated MSE values are quite small, and thus we conclude that the use of the linear mapping model is valid.

According to the image acquisition model [16, 17], the camera response corresponds to the integral of the product of the relative power spectral distribution of the reflected light and the spectral sensitivity function over all the wavelengths. Let us assume that the spectral sensitivity function used to capture the luminance plane of the visible color image can be approximated by scaling and translating the spectral sensitivity function of the near-infrared luminance image as follows:

$$S^v(\lambda) = \omega_1 R(\lambda) + \omega_2 G(\lambda) + \omega_3 B(\lambda) \quad (10)$$

$$\begin{aligned} \int S^v(\lambda) L(\lambda) d\lambda &\approx \int (\alpha S^{nir}(\lambda - \lambda_o) + \beta) L(\lambda) d\lambda \\ &= \alpha \left\{ \int S^{nir}(\lambda - \lambda_o) L(\lambda) d\lambda \right\} + \beta \left\{ \int L(\lambda) d\lambda \right\} \end{aligned} \quad (11)$$

where $R(\lambda)$, $G(\lambda)$, and $B(\lambda)$ denote the spectral sensitivity functions of a camera's filters that respond to the long, middle, and short visible wavelength regions, respectively. In addition, $L(\lambda)$ is the relative spectral power distribution of the reflected light, and $S^v(\lambda)$ and $S^{nir}(\lambda)$ correspond to the spectral sensitivity functions to capture the luminance plane of the visible color image and the near-infrared gray image, respectively. As shown in (10), the linear combination of $R(\lambda)$, $G(\lambda)$, and $B(\lambda)$ with weight ω generates the spectral sensitivity function $S^v(\lambda)$ to capture the luminance plane of the visible color image. If $S^v(\lambda)$ can be modeled by $\alpha S^{nir}(\lambda - \lambda_o) + \beta$, as shown in (11), where λ_o is a translation amount, the pixel value of the near-infrared gray image, described by $\int_\lambda S^{nir}(\lambda - \lambda_o) L(\lambda) d\lambda$, can be linearly mapped to the pixel value of the luminance plane of the visible color image, described by $\int_\lambda S^v(\lambda) L(\lambda) d\lambda$.

D. Detail Layer Transfer

The proposed contrast-preserving linear mapping enables the image appearance of the newly created near-infrared luminance plane to be similar to that of the luminance plane of the visible color image. Moreover, it can transfer the local contrast of the captured near-infrared luminance plane to the newly created near-infrared luminance plane. These results can be used to resolve the discrepancy mentioned in the introduction. Furthermore, the pixel saturation of the visible color image, as shown in Fig. 1(b), can be solved. However, when mapping the details of the near-infrared luminance plane to the luminance plane of the visible color image, some details can be lost. To address this issue, the detail layer of the newly created luminance plane is modified as follows:

$$\Delta \mathbf{x}^{d(l)} = \mathbf{x}^{d(l)} - \mathbf{x}^{b,d(l)} \quad \text{and} \quad \Delta \mathbf{x}^{nir} = \mathbf{x}^{nir} - \mathbf{x}^{b,nir} \quad (12)$$

$$\min_{\Delta \mathbf{x}} \left\{ \mu_d \|\Delta \mathbf{x} - \Delta \mathbf{x}^{d(l)}\|^2 + \sum_j^N \sum_{i=1}^N |(\Delta \mathbf{x} \otimes f^j)_i - (\Delta \mathbf{x}^{nir} \otimes f^j)_i| \right\} \quad (13)$$

$$\mathbf{x}^{o(l)} = \mathbf{x}^{b,d(l)} + \Delta \mathbf{x} \quad (14)$$

where $\mathbf{x}^{b,d(l)}$ and $\mathbf{x}^{b,nir}$ denote the base layers of the newly created near-infrared luminance plane and the captured near-infrared luminance plane, respectively, and $\Delta \mathbf{x}^{d(l)}$ and $\Delta \mathbf{x}^{nir}$ indicate the corresponding detail layers. As shown in (14), the newly estimated detail layer $\Delta \mathbf{x}$ is obtained via (13) and then added to the base layer $\mathbf{x}^{b,d(l)}$, thus producing the detail-enhanced version $\mathbf{x}^{o(l)}$. In (13), the second term brings the gradient difference between the two detail layers closer. This detail difference constraint further enhances the details of the newly created near-infrared luminance plane. In (12), the two base layers are generated. In this paper, a nonlocal means filtering was used [18]. Other filtering, e.g., bilateral filtering could be considered [19]. Equation (13) can be solved by the alternating minimization technique [6-8].

E. Color Transfer

In this section, we introduce a method to create colors in the detail-enhanced near-infrared luminance image $\mathbf{x}^{o(l)}$. Since the relation between the visible color and near-infrared luminance planes has been established, the unknown colors for the detail-enhanced near-infrared luminance image $\mathbf{x}^{o(l)}$ can be derived as follows:

$$\mathbf{x}_i^{o(c1)} = \mathbf{x}_i^{v(c1)} / \alpha_{i,1} \quad \text{and} \quad \mathbf{x}_i^{o(c2)} = \mathbf{x}_i^{v(c2)} / \alpha_{i,1} \quad (15)$$

where $\mathbf{x}_i^{v(c1)}$ and $\mathbf{x}_i^{v(c2)}$ represent the two chrominance planes of the visible color image defined in the decorrelated color space [12]. The above equation indicates that the unknown chrominance planes $\mathbf{x}_i^{o(c1)}$ and $\mathbf{x}_i^{o(c2)}$ for the detail-enhanced near-infrared luminance image $\mathbf{x}^{o(l)}$ can be obtained by dividing the chrominance planes for the visible color image by $\alpha_{i,1}$, the mapping relation. Equation (15) is derived from the contrast-preserving linear mapping, that is, $\mathbf{x}_i^{nir} \alpha_{i,1} \approx \mathbf{x}_i^v$, which reveals that the unknown chrominance planes for the detail-enhanced near-infrared luminance image can be defined as the contrast-enhanced version of the chrominance planes for the visible color image. By combining the luminance plane $\mathbf{x}^{o(l)}$ with the chrominance planes $\mathbf{x}^{o(c1)}$ and $\mathbf{x}^{o(c2)}$, the proposed method not only preserves the local contrasts and details of the near-infrared gray image, but also transfers the colors from the visible color image to the newly created near-infrared luminance image.

F. Proposed Color Transfer vs. Chroma Mapping

The proposed color transfer, as given in (15), can be regarded as a chroma mapping [20]. In the CIELAB color space, the chroma value of the newly created colored image at the i th pixel location can be defined as:

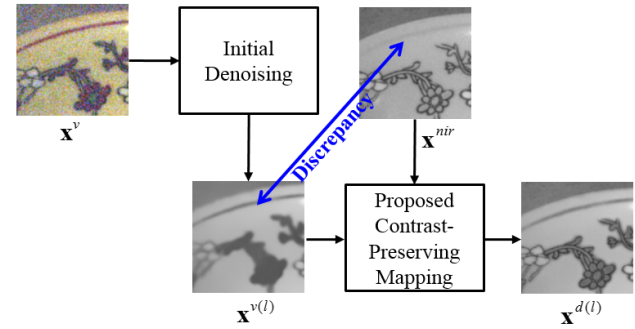


Fig. 3. Proposed scheme for near-infrared denoising.

$$C_i^* = \sqrt{\left(\mathbf{x}_i^{v(c1)} / \alpha_{i,1}\right)^2 + \left(\mathbf{x}_i^{v(c2)} / \alpha_{i,1}\right)^2} \\ = 1/\alpha_{i,1} \sqrt{\left(\mathbf{x}_i^{v(c1)}\right)^2 + \left(\mathbf{x}_i^{v(c2)}\right)^2} = s_i \sqrt{\left(\mathbf{x}_i^{v(c1)}\right)^2 + \left(\mathbf{x}_i^{v(c2)}\right)^2} \quad (16)$$

where C_i^* is the chroma value. The above equation reveals that the proposed color transfer model linearly changes the chroma value of the captured visible color image \mathbf{x}_i^v according to the inverse number of the local contrast $\alpha_{i,1}$. If $1/\alpha_{i,1}$ is generalized to a scaling factor s_i , (16) becomes the same as space-variant chroma mapping. Therefore, it is expected that the effectiveness of the proposed color transfer is similar to that of the chroma mapping.

G. Parameter Setting

In this paper, two parameters μ_c and μ_d are determined empirically. In (4), if the value of μ_c is zero, the near-infrared patch is almost the same as the visible luminance patch. It means that any local contrasts of the near-infrared patch are not transferred into the visible luminance patch. On the other hand, if the value of μ_c approaches to infinity, the estimated μ_c will become equal to the local contrast α_0 . Therefore, the newly generated near-infrared gray image looks like a contrast map. In this study, μ_c is determined empirically. Our experiments show that $\mu_c = 7500$ can transfer the local contrasts of the near-infrared patches into the visible luminance patches. Similarly, the value of μ_d is set with 200 to transfer the detail layer of the captured near-infrared image into the detail layer of the newly generated near-infrared image. In the paper, μ_c and μ_d are fixed for all test images.

IV. PROPOSED NEAR-INFRARED DENOISING

In dim lighting conditions, visible color images may contain noise. Even in this case, the proposed approach for near-infrared coloring can be directly applied to the captured image pair of the noise-contained visible color image and the near-infrared gray image; only an initial denoising is required. That is, the proposed coloring method can be directly applied to the image pair of the denoised visible color image and the near-infrared gray image. The initial denoising can remove fine details in the visible color image along with the noise. However, the proposed contrast-preserving mapping can transfer the

details of the captured near-infrared gray image to the newly created near-infrared gray image. Therefore, the newly created near-infrared gray image can be both noise-free and detail-preserved. Moreover, the discrepancy between the noisy visible color image and near-infrared gray image can be resolved via the proposed contrast-preserving mapping.

Fig. 3 shows how the proposed near-infrared coloring method can deal with the noise and discrepancy issues. First, to remove the noise in the visible color image, an initial denoising is performed. It is recommended that the noise be completely removed, as shown in the denoised gray image $\mathbf{x}^{v(l)}$. Second, to restore the image structure of the denoised gray image $\mathbf{x}^{v(l)}$, the proposed contrast-preserving mapping is used. The proposed contrast-preserving mapping can transfer details from the captured near-infrared gray image \mathbf{x}^{nir} to the denoised gray image $\mathbf{x}^{v(l)}$, as shown in the newly created near-infrared gray image $\mathbf{x}^{d(l)}$. Moreover, the discrepancy between $\mathbf{x}^{v(l)}$ and \mathbf{x}^{nir} that can be found in the red lines near the brim can be resolved at the same time. The unknown colors can then be added to the newly created near-infrared gray image $\mathbf{x}^{d(l)}$ according to the color transfer model in (15). Thus, the proposed near-infrared denoising method is similar to a coloring method. This is because details and colors are transferred to the denoised gray image $\mathbf{x}^{v(l)}$. This is a main difference between the proposed near-infrared denoising and conventional-image-pair-based fusions via gradient regularization [3,6,7], weighted least squares [2], and multiresolution [1,9,10] methods.

V. EXPERIMENTAL RESULTS

A. Visual Quality Comparison

To verify the visual effectiveness of the proposed coloring method, test images that include high contrast and details are chosen from the near-infrared image database [1], as shown in Figs. 4, 5, 6, and 7. Also, to compare the performance of the proposed method, the conventional image fusion techniques such as the gradient regularization [3,6,7], multiresolution [1, 9,10], and multiscale tone and detail manipulation [4] are adopted because the near-infrared coloring can be considered as an image fusion problem. Note that the proposed coloring method is good at representing local detail, contrast, and realistic colors. As shown in Fig. 4(a), the newly created near-infrared luminance image, rendered using (4), preserves detail in the tree regions. Furthermore, the tree regions that are darkened in the visible color image because of the low dynamic range of the camera, as depicted in Fig. 1(b), can be recovered with higher contrast. However, details can be lost when mapped from the near-infrared gray image into the luminance plane of the visible color image. For example, the lines on the wall in the highlight regions are almost lost. However, this drawback can be overcome via the detail layer transfer of Eqs. (12)-(14). In Fig. 4(b), the lines on the wall are restored. In addition, the details of the tree's leaves and road surfaces are also enhanced. For comparison, magnified versions of the red rectangles marked in Figs. 4(a), 5(c), and 6(c) are shown in Fig. 8. From these results, it can be concluded that the detail layer transfer improves the amount of information and detail description. The

naive coloring method of combining the chrominance planes of the visible color image with the newly created near-infrared luminance image resulted in improved colors, as shown in Fig. 4(c). The colors are more natural than those of Fig. 1(c), indicating that the discrepancy problem can be resolved by the proposed contrast-preserving mapping. However, the color appears desaturated. The proposed color-transfer method, as defined in (15), improved the color by estimating the contrast-enhanced version of the chrominance planes for the visible color image, as shown in Fig. 4(d). In addition, the colors produced with the proposed coloring method are better than those resulting from conventional methods, as shown in Figs. 4(e)-(h). The difference between Figs. 4(e) and 4(f) depends on the value of μ_g defined in (1). A lower value enables the preservation of the edges from the near-infrared gray image. Despite an increase in the edges of the tree regions, the colors become distorted, as shown in Fig. 4(f). The multiresolution approach, shown in Fig. 4(g), preserves the details but results in unnatural colors. The dehazing technique [4] cannot solve the discrepancy problem. The brightness of the tree's regions is still dark and some lines on the wall are almost removed, as shown in Fig. 4(h). The statistical approach [12] is not compared in this paper, because its visual qualities are no better than those of the gradient regularization, dehazing, and multiresolution approaches. In particular, the colors it produced are unnatural and oversaturated.

Similar effects can be found in Figs. 5 and 6. It can be seen that the discrepancy problem occurs, especially in the grass region of Figs. 5(a) and (b) and the cloud region of Figs. 6(a) and (b). Unnatural colors are produced by the naive coloring method, as shown in Figs. 5(g) and 6(g). In Figs. 5(f) and 6(f), the proposed method produces better colors than the naive gradient regularization, multiresolution, and dehazing approaches. Note that the conventional methods have their own merits. The gradient regularization approach is good at the representing edges, as shown in the grass region of Fig. 5(h) and the bush region of Fig. 6(h). In contrast, the multiresolution approach is good at increasing the amount of visual information, especially in the distant mountain region of Fig. 5(i) and the cloud region of Fig. 6(i). The disadvantage to use the gradient regularization approach is that it often omits visual information. For example, the cloud in the sky is removed, as shown in Fig. 6(h). The disadvantage of the multiresolution approach is that the colors it produces are often unrealistic, as shown in Fig. 5(i), and the strength of edges are relatively weak when compared to the gradient regularization and proposed method, as in the roof regions of Fig. 6(i). The advantage and disadvantage of the dehazing approach [4] are similar to those of the multiresolution approach, as checked in Figs. 5(j) and 6(j). This is because the dehazing method is based on the multiscale tone and detail manipulation. Thus, both the proposed and conventional methods have their own pros and cons. However, the proposed method is more effective at expressing the color contrasts than conventional methods. In addition, fine details and natural colors can be obtained simultaneously. It is possible because the proposed coloring method adopts three kinds of transfer: contrast, detail, and color, as shown in the

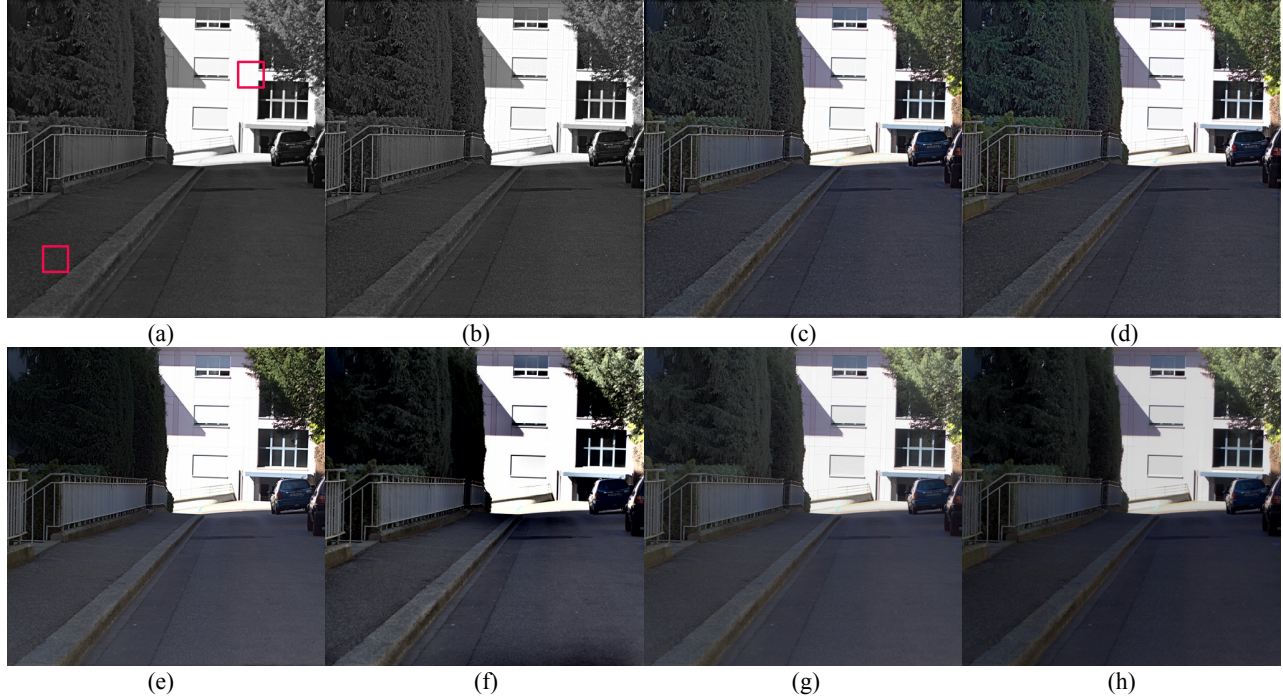


Fig. 4. Experimental results: (a) newly created near-infrared gray image using the proposed contrast-preserving mapping, (b) the same image with details enhanced using the proposed detail layer transfer method, (c) detail enhanced image colored by the naive method, (d) detail enhanced image colored by the proposed color-transfer method, (e) near-infrared image colored by the gradient regularization approach ($\mu_g = 10^3$), (f) near-infrared image colored by the gradient regularization approach ($\mu_g = 1$), (g) near-infrared image colored by the multiresolution approach, (h) near-infrared image colored by the dehazing technique [4].

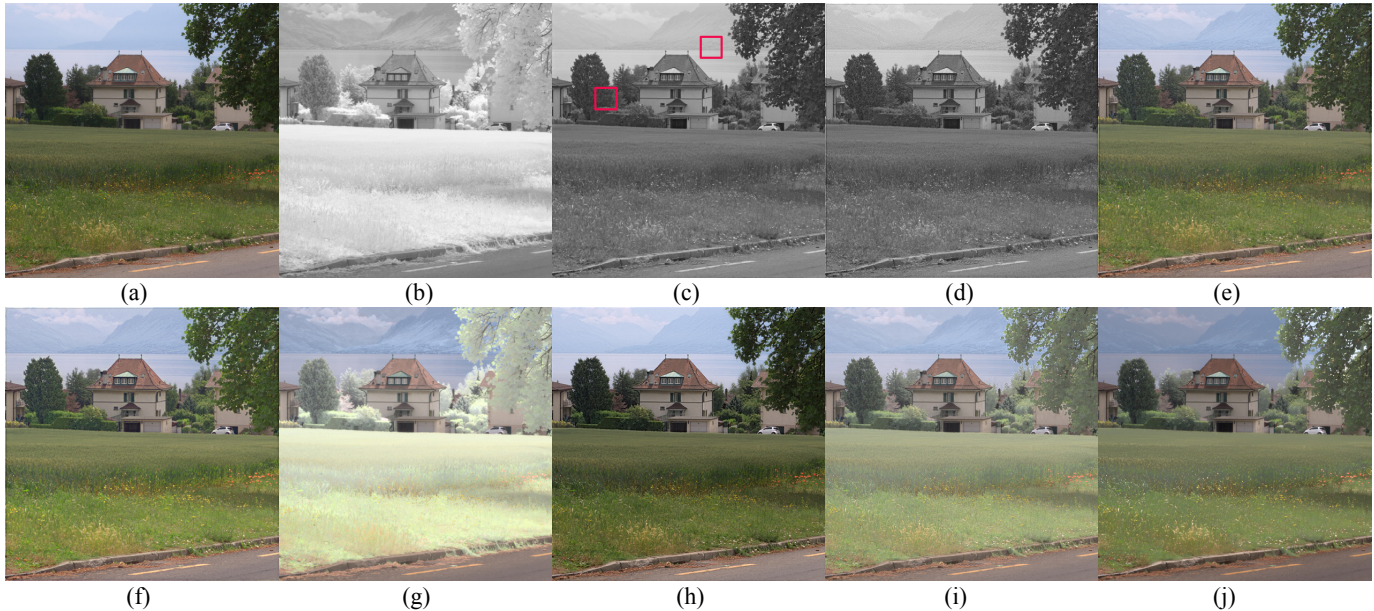


Fig. 5. Experimental results: (a) visible color image, (b) near-infrared gray image, (c) newly created near-infrared gray image using the proposed contrast-preserving mapping, (d) newly created near-infrared gray image with details enhanced using the proposed detail layer transfer method, (e) detail enhanced image colored by naive method, (f) detail enhanced image colored by the proposed color-transferring method, (g) near-infrared image colored by the naive method, (h) near-infrared image colored by the gradient regularization approach ($\mu_g = 10^3$), (i) near-infrared image colored by the multiresolution approach, and (j) near-infrared image colored by the dehazing technique [4].

block-diagram of Fig. 2. In addition, the proposed method put more emphasis on near-infrared coloring, whereas the conventional methods focus on fusing the images for the improvement of edge representation and information preservation. This is the main difference between the proposed

and conventional methods. For a more visual comparison, additional image results are provided in Fig. 7. Moreover, a few visible/near-infrared image sets including thin lines and high texture content are tested, and then provided in supplementary material. The performance results are similar to Figs. 4-7.

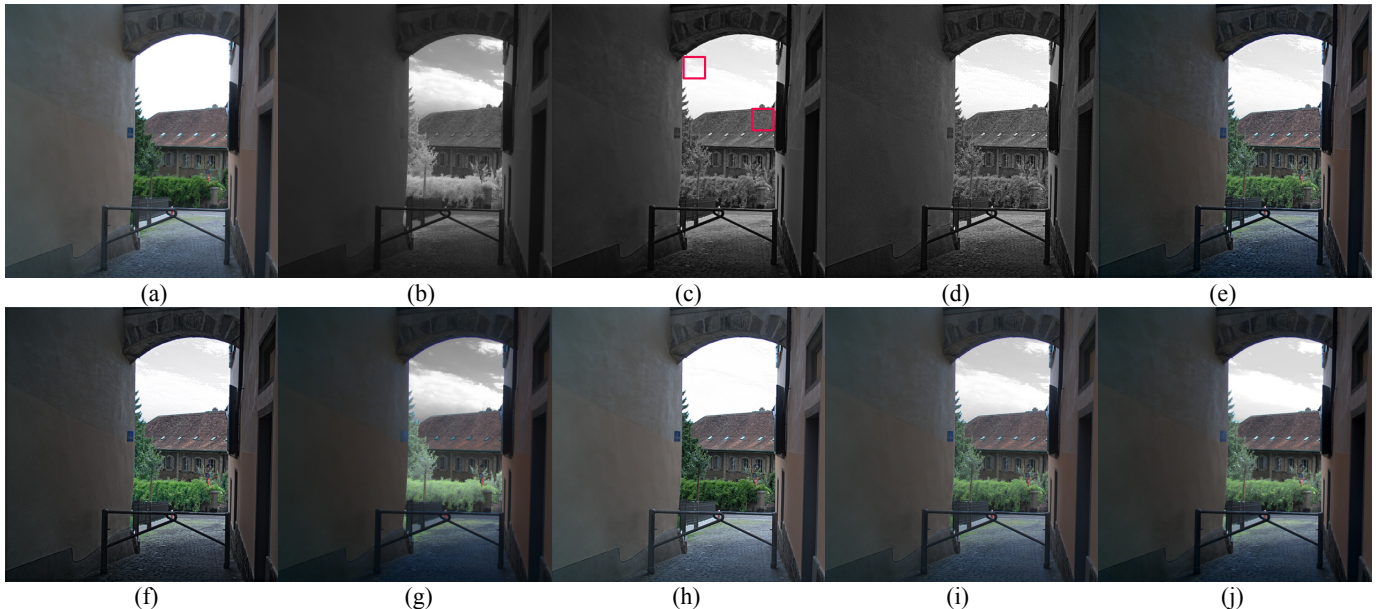


Fig. 6. Experimental results: (a) visible color image, (b) near-infrared gray image, (c) newly created near-infrared gray image with the proposed contrast-preserving mapping, (d) newly created near-infrared gray image with details enhanced using the proposed detail layer transfer method, (e) detail enhanced image colored by the naive method, (f) detail enhanced image with the proposed color-transferring method, (g) near-infrared image colored by the naive method, (h) near-infrared image colored by the gradient regularization approach ($\mu_g = 10^3$), (i) near-infrared image colored by the multiresolution approach, and near-infrared image colored by the dehazing technique [4].



Fig. 7. Experimental results: visible color images (first column), near-infrared gray images (second column), and images colored by the proposed method (third column), naive method (fourth column), gradient regularization approach (fifth column), multiresolution approach (sixth column), and dehazing technique [4] (seventh column).

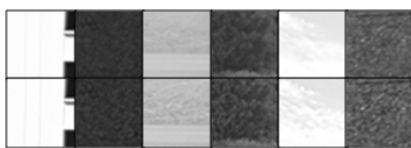


Fig. 8. Detail comparison: before detail layer transfer (upper row) and after detail layer transfer (bottom row).

B. Quantitative Evaluation

To evaluate the performance of the coloring methods, four types of measures: colorfulness (CF) [21], spatial frequency

(SF) [22], entropy (EN) [23], and contrast (CT) [14,15] are employed. These measures are defined in Table II. These four measures have been used for the quantitative evaluation of other types of image pairs [23]. In this paper, the CF measure is used to perceptually quantify the colorfulness in a colored image and the SF measure is used to measure edge preservation. The EN and CT measures quantify the amount of information and local contrast in a colored image, respectively. At least one of the contrast, edge, color, or visual information can be lost after applying image fusion including the near-infrared coloring. Therefore, we use these four measures to evaluate the near-infrared coloring because it is necessary to measure

TABLE II
DEFINITIONS OF THE FOUR MEASURES

$CF = \sigma_{ab} + 0.94u_C$, where σ_{ab} and u_C are related to the standard deviation of the chrominance planes and mean value of the chroma image, respectively.
$SF = \sqrt{R_F^2 + C_F^2}$, where R_F and C_F indicate the averaged numbers of the vertical and horizontal edges, respectively.
$EN = -\sum_{i=1}^L h(i) \log h(i)$, where h indicates the normalized histogram of a colored image.
$CT = \frac{1}{N} \sum_{i=1}^N \left \mathbf{x}_i^o - (\mathbf{x}^o \otimes \mathbf{k})_i \right $, where \mathbf{k} indicates a Gaussian filter.

TABLE III
QUANTITATIVE EVALUATION

Test Images	Measures	CT	EN	SF	CF
	Methods				
Fig. 4	Naive method	12.949	14.623	15.749	11.891
	Gradient regularization	17.375	14.770	23.367	11.893
	Multi-resolution	14.516	14.761	18.68	11.936
	Dehazing method [4]	13.070	14.552	16.863	12.394
	Proposed method	19.046	14.846	23.675	13.732
Fig. 5	Naive method	13.828	15.625	15.219	28.583
	Gradient regularization	19.503	15.742	22.5	31.487
	Multi-resolution	16.356	15.497	18.711	29.781
	Dehazing method [4]	16.112	15.261	19.367	30.946
	Proposed method	20.111	15.704	23.445	38.373
Fig. 6	Naive method	8.512	14.322	9.797	11.317
	Gradient regularization	12.991	14.302	17.159	11.052
	Multi-resolution	10.603	14.423	13.54	11.133
	Dehazing method [4]	10.857	14.314	12.999	11.208
	Proposed method	13.741	14.555	17.845	10.366
Fig. 7 (First row)	Naive method	10.657	14.826	10.98	16.397
	Gradient regularization	12.909	15.113	14.128	17.604
	Multi-resolution	10.995	14.945	11.616	16.914
	Dehazing method [4]	12.157	15.033	12.447	17.114
	Proposed method	14.656	15.138	15.787	21.759
Fig. 7 (Second row)	Naive method	19.025	15.410	17.031	17.164
	Gradient regularization	19.464	14.895	17.122	17.483
	Multi-resolution	18.158	15.083	16.798	17.685
	Dehazing method [4]	12.874	15.105	15.962	17.925
	Proposed method	23.630	15.205	20.238	30.029
Fig. 7 (Third row)	Naive method	24.637	15.944	24.751	21.608
	Gradient regularization	33.450	15.922	36.554	22.587
	Multi-resolution	27.209	15.893	28.758	22.623
	Dehazing method [4]	25.785	15.795	27.206	22.702
	Proposed method	31.207	15.889	34.068	24.579
AVG.	Naive method	14.935	15.125	15.588	17.827
	Gradient regularization	19.282	15.124	21.805	18.684
	Multi-resolution	16.306	15.100	18.017	18.345
	Dehazing method [4]	15.143	15.010	17.474	18.715
	Proposed method	20.399	15.223	22.510	23.190

how well the contrast, edge, color, and visual information are represented on the fused or colored images. Image quality measures that require a reference image [23] are not considered in this paper because both visible color and near-infrared gray images can contain image quality degradation, and thus neither can be used as the reference image. For example, as shown in

Figs. 1(a) and (b), the visible color image includes contrast loss and the near-infrared gray image has no color. Thus, reference image fusion metrics, such as the root mean square error (RMSE) or peak signal to noise ratio (PSNR), are not considered. Even though there are some blind image quality evaluations where natural statistics of edges, colors, or

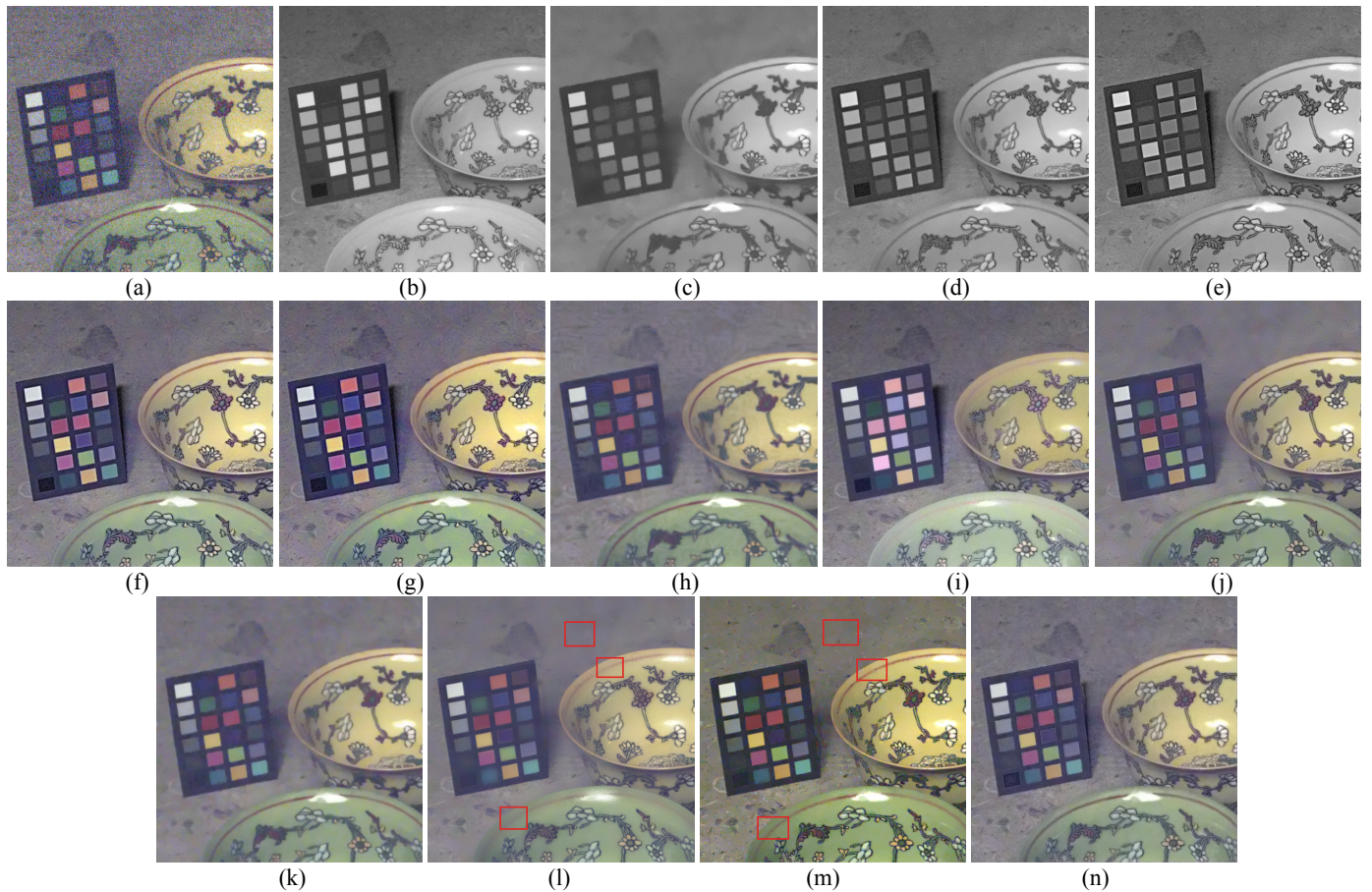


Fig. 9. Experimental results for noise removal: (a) noisy visible color image, (b) near-infrared gray image, (c) image denoised via nonlocal means filtering [18], (d) newly created near-infrared gray image via the proposed contrast-preserving mapping, (e) newly created near-infrared gray image with details enhanced using the proposed detail layer transfer method, (f) image colored using the proposed color transfer method, (g) chroma-enhanced version of the Fig. 9(f), (h) image denoised using BM3D [26], (i) image colored by the naive method, (j) image denoised using the gradient regularization approach, (k) image denoised using the weighted least squares approach, (l) image denoised using guided image filtering [27], (m) image denoised using scale map method [28], and (n) image denoised using layer decomposition [29].

contrasts are modeled to predict distortion levels [24], image enhancement algorithms such as sharpening, haze removal, coloring, or etc., lead to inevitable modification in the natural statistics. Thus, the blind image quality evaluation is not appropriate for near-infrared coloring.

As expected, the naive coloring method yields the lowest average scores, as shown in the lowest partition of Table III. However, the EN score is relatively high, especially for the test images located in the second and third rows of Fig. 7. The EN measure has the highest score when a discrete random variable has a uniform probability distribution [25], i.e., when the histogram of an image is uniform. Because these two test images have a wide range of pixel intensities, they obtained the highest EN scores. The gradient regularization approach is good at representing edges, and thus it obtains higher SF scores, especially for the test image of Fig. 7 (third row). A small value of μ_g in (1) can increase the SF scores, however color distortion can occur, as shown in Figs. 4(e) and (f). In contrast, the proposed method obtains the highest average scores for all evaluations, as shown in the lowest partition of Table III. This is due to three types of transfer: contrast-preserving mapping, detail layer transfer, and color transfer. The contrast-

preserving mapping preserves the local contrast of the near-infrared gray image and the color transfer increases the chrominance range of the visible color image. The detail layer transfer increases the strength of details and edges. The perceptual meaning of the CF score (the final column of Table III) is introduced in [21]. For example, a score that lies between 8 and 18 indicates that a tested image is slightly colorful and a score between 32 and 43 indicates that a tested image is quite colorful. Note that the proposed method obtains higher CF scores for the colorful images of Figs. 5 and 7 (second row). In Table III, the quantitative evaluations of the multiresolution and dehazing approaches are not satisfactory. However, specific areas in the whole images, e.g., sky regions, can be well rendered. This indicates that those two approaches are more appropriate for dehazing [4], not the near-infrared coloring [1].

C. Application of Proposed Coloring Method for Denoising, Dehazing, and Local Contrast Enhancement

In this section, it is shown how effectively the proposed near-infrared coloring method can be used for noise and haze removal, as well as local contrast enhancement. First, as shown in the block-diagram of Fig. 3, the proposed method can be



Fig. 10. Experimental results for haze removal; captured visible color images (first row), captured near-infrared images (second row), dehazed images by using the conventional method based on multiscale fusion [30] (third row), dehazed images by using the near-infrared dehazing method [31] (fourth row), and **colored near-infrared images with the proposed method** (fifth row).

used with a little modification for noise removal. Fig. 9 shows the experimental results for the captured near-infrared images in dim lighting [2]. In Figs. 9(a) and (b), it is clear that the visible color image contains noise and discrepancy occurs, especially for the chart's patches and red lines near the brim of

the bowl. Fig. 9(c) shows the initially denoised visible color image via nonlocal means filtering [18]. In this figure, the details have clearly been removed. However, this detail loss can be restored by applying the proposed contrast-preserving mapping and detail layer transfer, as shown in Figs. 9(d) and (e).



Fig. 11. Experimental results for local contrast enhancement; contrast-enhanced images with the adaptive histogram equalization [33] (first column), contrast-enhanced image via a retinex model [34] (second column), **contrast-enhanced image with proposed coloring method (last column)**.

In Fig. 9(d), it is clear that the newly created near-infrared gray image preserves its details, thanks to the proposed contrast-preserving mapping. Moreover, the discrepancy problem can be resolved. For example, the red line on the bowl that was removed in the near-infrared gray image of Fig. 9(b) is restored. In Fig. 9(e), the use of the detail layer transfer leads to an improvement in the detail description. Fig. 9(f) shows the colored image with the proposed color transfer method and Fig. 9(g) is the chroma-enhanced version of the Fig. 9(f). That is, the chroma mapping, as shown in (16), is applied to the Fig. 9(f). The scale factor, s_i , is set to 1.2. In the case of the noisy visible and near-infrared image pairs, the values of the estimated linear mapping relation, α_i , in (4), can be shrunk. It is because the used denoised luminance image has already lost its contrast and edge, as shown in Fig. 9(c), which can lead to the decrease in chroma. Different from other resulting images, as shown in Figs. 9(h)-(m), the colored image with the proposed denoising method has little noise and color distortions. Thus, the chroma mapping can improve the colorfulness without noise amplification, as shown in Fig. 9(g). BM3D [26] is a state-of-the-art denoising method. However, its visual quality is poor, as shown in Fig. 9(h). It is possibly due to the non-Gaussian noise in the captured visible color image. The image-pair-based denoising methods based on the weighted least squares [2] and gradient regularization [3,6,7] can produce better-resulting images than those obtained from the BM3D. It is because the clean near-infrared image is used as a guidance

image [2]. Figs. 9(l) and (m) show the denoised images with the guided image filtering [27] and scale map method [28], respectively. As shown in the red boxes of Fig. 9(l), the lines cannot be restored. Also, the background textures are almost removed. It shows that the guided image filtering is not suitable for resolving the discrepancy problem. Similarly, the scale map method cannot clearly restore the lines, as shown in red boxes. The edges of the brim of the bowl are broken. Also, the background colors are different from those of the captured visible color image. Even though the layer decomposition method [29] is strong at the texture representation, the overall sharpness needs to be improved, compared to the proposed method. In addition, the layer decomposition method is quite slow, due to the repetition of the used sparse coding. Based on the comparison of resulting images, the visual quality of the proposed method is better than those of the conventional methods. It is because the proposed denoising method is based on both detail and color transfers, as discussed in Section IV. In other words, the proposed denoising method adds details and colors to the denoised luminance image of Fig. 9(c). This is a main difference between the proposed denoising method and the conventional image fusion methods [2,3,27,28]. From these results, it can be concluded that the proposed near-infrared coloring method is effective to remove noise of the captured visible color images in dim lighting conditions.

In Fig. 9, it is noted that the weighted least squares and gradient regularization approaches utilize both the noisy visible color image and near-infrared gray image. The denoised

version of the noisy visible color image via the nonlocal means denoising is used as a guidance image in the weighted least squares approach [2]. The gradient regularization approach use the denoised image to model the data-fidelity term, as shown in (1). Therefore, the weighted least squares and gradient regularization approaches can be considered as multi-frame denoising methods as well.

Second, the proposed method can also be used effectively for haze removal and local contrast enhancement. As shown in Fig. 10, the conventional multiscale-based fusion [30] cannot remove the haze. This is because the captured visible color images have already lost detail and edge information during image capturing, due to heavy haze. The near-infrared dehazing method [31] uses the near-infrared gray images as guidance images to enhance the edges of the initial dehazed images, which are given by the dark prior method [32]. However, haze still remains on the dehazed images even though the overall sharpness can be improved, as shown in the fourth row. In addition, the visual quality is no better than the proposed method. The proposed coloring method can solve serious discrepancy in the image structure and brightness between the captured haze images and the near-infrared gray images, and thus the proposed method can remove heavy haze and produce natural-looking colors, indicating that the proposed near-infrared coloring is more effective in removing haze and producing natural colors than conventional dehazing methods.

Fig. 11 shows the experimental results for local contrast enhancement. As shown in the first column, adaptive histogram equalization method [33] can improve local contrast. However, this method cannot restore the lines on the building. Also, the produced colors are poor. The retinex-based contrast enhancement [34] can improve visual quality compared to the adaptive histogram equalization method, as shown in the second column, but it cannot restore the lines. In contrast, the proposed coloring method can restore the lines on the building and provide more visual information, as shown in red boxes. Even though the retinex-based contrast enhancement [34] is good at describing local contrasts, there is some room in improvement in terms of the produced colors and shading. These results show that the proposed coloring method is effective in improving local contrasts and colors.

VI. CONCLUSION

In this paper, a new method is presented to transfer colors from a visible color image to a near-infrared gray image without losing details and contrast. Specifically, based on a new contrast-preserving mapping model, the proposed contrast-preserving mapping method can solve the discrepancy problem in brightness and image structures between the visible and near-infrared images. Visual information loss during the contrast-preserving mapping can be compensated by the transfer of image details, thereby restoring thin lines and improving fine details. In addition, dehazing effects can be simultaneously obtained through the proposed contrast-preserving mapping model and the detail transfer procedure. The proposed color-transfer technique generates realistic colors that can be added to the newly created near-infrared gray image

by applying the space-variant chroma mapping to the chrominance planes of the captured visible color image. The proposed approach for the near-infrared coloring can also be used to remove noise in visible color image captured in dim lighting condition, as well as haze removal and contrast enhancement. Experimental results show the effectiveness and superiority of the new method in comparison with other commonly used methods.

REFERENCES

- [1] C. Fredembach and S. Susstrunk, "Colouring the near infrared," in *Proc. IS&T Color Imaging Conference*, Los Angeles, California, U.S.A., 2008, pp. 176-182.
- [2] S. Zhuo, X. Zhang, X. Miao, and T. Sim, "Enhancing low light images using near infrared flash image," in *Proc. IEEE International Conference on Image Processing*, Hong Kong, 2010, pp. 2537-2540.
- [3] W. Lia, J. Zhang, and Q.-H. Daib, "Robust blind motion deblurring using near-infrared flash image," *Journal of Visual Communication and Image Representation*, vol. 24, no. 8, pp. 1394-1413, Nov. 2013.
- [4] L. Schaul, C. Fredembach, and S. Susstrunk, "Color image dehazing using the near-infrared," in *Proc. IEEE International Conference on Image Processing*, Cairo, Egypt, 2009, pp. 1629-1932.
- [5] S. Farokhi, S. M. Shamsuddin, U. U. Sheikh, J. Flusser, M. Khansari, and K. Jafari-Khouzani, "Near infrared face recognition by combining Zernike moments and undecimated discrete wavelet transform," *Digital Signal Processing*, vol. 31, pp. 13-27, Aug. 2014.
- [6] S.-H. Lee, H.-M. Park, and S.-Y. Hwang, "Motion deblurring using edge map with blurred/noisy image pairs," *Optics Communications*, vol. 285, no. 7, pp. 1777-1786, Apr. 2012.
- [7] S. Zhuo, D. Guo, and T. Sim, "Robust flash deblurring," in *Proc. IEEE International Conference on Computer Vision and Pattern Recognition*, San Francisco, CA, U.S.A., 2010, pp. 2440-2447.
- [8] C.-H. Son, H. Choo, and H.-M Park, "Image-pair-based deblurring with spatially varying norms and noisy image updating," *Journal of Visual Communication and Image Representation*, vol. 24, no. 8, pp. 1303-1315, Nov. 2013.
- [9] M. Tico and K. Pulli, "Image enhancement method via blur and noisy image fusion," in *Proc. IEEE International Conference on Image Processing*, Cairo, Egypt, 2009, pp. 1521-1524.
- [10] V. S. Petrovic and C. S. Xydeas, "Gradient-based multiresolution image fusion," *IEEE Transactions on Image Processing*, vol. 13, no. 2, pp. 228-237, Feb. 2004.
- [11] C.-H. Son and X.-P. Zhang, "Near-infrared coloring via a contrast preserving mapping model," in *Proc. IEEE Global Conference on Signal & Information Processing*, Orlando, USA., pp. 677-681, Dec. 2015.
- [12] E. Reinhard, M. Ashikhmin, B. Gooch, and P. Shirley, "Color transfer between images," *IEEE Computer Graphics and Application*, vol. 21, no. 5, pp. 34-41, Sep./Oct. 2001.
- [13] C.-H. Son and H. Choo, "Local learned dictionaries optimized to edge orientation for inverse halftoning," *IEEE Transactions on Image Processing*, vol. 23, no. 6, pp. 2542-2556, June 2014.
- [14] Z. Rahman, D. J. Jobson, G. A. Woodell, "Retinex processing for automatic image enhancement," *Journal of Electronic Imaging*, vol. 13, no. 1, pp. 100-110, Jan. 2004.
- [15] G. Simone, M. Pedersen, and J. Y. Hardeberg, "Measuring perceptual contrast in digital images," *Journal of Visual Communication and Image Representation*, vol. 23, no. 3, pp. 491-506, Apr. 2012.
- [16] K. Barnard and B. Funt, "Camera characterization for color research," *Color Research and Application*, vol. 27, no. 3, pp. 152-163, June 2002.
- [17] C.-H. Son and Y.-H. Ha, "Color correction of images projected on a colored screen for mobile beam projector," *Journal of Imaging Science and Technology*, vol. 52, no. 3, pp. 030505-030505-11, May-Jun. 2008.
- [18] A. Buades, B. Coll, and J.-M. Morel, "A non-local algorithm for image denoising," in *Proc. IEEE International Conference on Computer Vision and Pattern Recognition*, San Diego, CA, U.S.A., 2010, pp. 2537-2540.
- [19] C. Tomasi and R. Manduchi, "Bilateral filtering for gray and color Images," in *Proc. IEEE International Conference on Computer Vision*, Bombay, India, 1998, pp. 839-846.
- [20] E. D. Montag and M. D. Fairchild, "Psychophysical evaluation of gamut mapping techniques using simple rendered images and artificial gamut

- boundaries," *IEEE Transactions on Image Processing*, vol. 6, no. 7, pp. 977-988, July 1997.
- [21] D. Hasler and S. Susstrunk, "Measuring colourfulness in natural images," in *Proc. IS&T/SPIE Electronic Imaging 2003: Human Vision and Electronic Imaging VIII*, vol. 5007, San Jose, CA, U.S.A., pp. 87-95.
- [22] S. Li and B. Yang, "Multifocus image fusion by combining curvelet and wavelet transform," *Pattern Recognition Letters*, vol. 29, no. 9, pp. 1295-1301, July 2008.
- [23] M. Bagher, A. Haghigat, A. Aghagolzadeh, and H. Seyedarabi, "A non-reference image fusion metric based on mutual information of image features," *Computers and Electrical Engineering*, vol. 37, no. 5, pp. 744-759, Sept. 2011.
- [24] L. Zhang, L. Zhang, and A. C. Bovik, "A feature-enriched completely blind image quality evaluator," *IEEE Transactions on Image Processing*, vol. 24, no. 8, pp. 2579 - 2591, Aug. 2015.
- [25] C. M. Bishop, *Pattern recognition and machine learning*, Springer, 2006.
- [26] K. Dabov, A. Foi, V. Katkovnik, and K. Egiazarian, "Image denoising by sparse 3D transform-domain collaborative filtering," *IEEE Transactions on Image Processing*, vol. 16, no. 8, pp. 2080 – 2095, Aug. 2007.
- [27] K. He, J. Sun, and X. Tang, "Guided image filtering," in *Proc. European Conference on Computer Vision*, 2010, pp. 1-14.
- [28] Q. Yan, X. Shen, L. Xu, S. Zhuo, X. Zhang, L. Shen, and Jiaya Jia, "Cross-field joint image restoration via scale map," in *Proc. IEEE International Conference on Computer Vision*, 2013, pp. 1537-1544.
- [29] C.-H. Son and X.-P. Zhang, "Layer-based approach for image pair fusion," *IEEE Transactions on Image Processing*, vol. 25, no. 6, pp. 2866-2881, June 2016.
- [30] C. O. Ancuti and C. Ancuti, "Single image dehazing by multi-scale fusion," *IEEE Transactions on Image Processing*, vol. 22, no. 8, pp. 3271-3282, Aug. 2013.
- [31] C. Feng, S. Zhuo, X. Zhang, L. Shen, and S. Susstrunk, "Near-infrared guided color image dehazing," in *Proc. IEEE International Conference on Image Processing*, Melbourne, Australia, 2013, pp. 2363- 2367.
- [32] K. He, J. Sun, and X. Tang, "Single image haze removal using dark channel prior," in *Proc. IEEE International Conference on Computer Vision and Pattern Recognition*, Miami, FL, USA, 2009, pp. 1956-1963.
- [33] K. Zuiderveld, "Contrast limited adaptive histogram equalization." *Graphic Gems IV*. San Diego: Academic Press Professional, 1994. pp. 474-485
- [34] C.-T. Shen and W.-L. Hwang, "Color image enhancement using retinex with robust envelope," in *Proc. IEEE International Conference on Image Processing*, Cairo, Egypt, 2009, pp. 3141-3144.



Chang-Hwan Son received the B.S., M.S., and Ph.D. degrees in Electronic Engineering from Kyungpook National University, Daegu, Korea, in 2002, 2004, and Aug. 2008, respectively. He was a National Scholarship Student in 2006. From 2008 to 2009, he was with the Advanced Research and Development Group 2, Digital Printing Division, Samsung Electronics Company, Ltd., Suwon, Korea. As a Senior Research Engineer, he was involved in the development of color reproduction algorithms in digital printers and copiers. From Mar. 2015 to Feb. 2017, he was a postdoctoral researcher with the Department of Electrical and Computer Engineering, Ryerson University, Canada. He is now Assistant Professor of the Department of the Software Convergence Engineering, Kunsan National University, South Korea. His main research interests include color imaging, computational photography, learning representation, image processing, sparse representation, printing, and hardcopy watermarking. He was a reviewer of the *IEEE Transactions on Image Processing*, *IEEE Transactions on Multimedia*, *IEEE Transactions on Circuits and Systems for Video Technology*, *SIAM Journal on Imaging Sciences*, and *IEEE Signal Processing Letters*.

digital printers and copiers. From Mar. 2015 to Feb. 2017, he was a postdoctoral researcher with the Department of Electrical and Computer Engineering, Ryerson University, Canada. He is now Assistant Professor of the Department of the Software Convergence Engineering, Kunsan National University, South Korea. His main research interests include color imaging, computational photography, learning representation, image processing, sparse representation, printing, and hardcopy watermarking. He was a reviewer of the *IEEE Transactions on Image Processing*, *IEEE Transactions on Multimedia*, *IEEE Transactions on Circuits and Systems for Video Technology*, *SIAM Journal on Imaging Sciences*, and *IEEE Signal Processing Letters*.



Xiao-Ping Zhang (M'97, SM'02) received B.S. and Ph.D. degrees from Tsinghua University, in 1992 and 1996, respectively, both in Electronic Engineering. He holds an MBA in Finance, Economics and Entrepreneurship with Honors from the University of Chicago Booth School of Business, Chicago, IL. Since Fall 2000, he has been with the Department of Electrical and Computer Engineering, Ryerson University, where he is now Professor, Director of Communication and Signal Processing Applications Laboratory (CASPAL). He has served as

Program Director of Graduate Studies. He is cross appointed to the Finance Department at the Ted Rogers School of Management at Ryerson University. He was Visiting Scientist at Research Laboratory of Electronics (RLE), Massachusetts Institute of Technology, in 2015 and 2017. His research interests include image and multimedia content analysis, statistical signal processing, sensor networks and electronic systems, machine learning, and applications in big data, finance, and marketing. He is a frequent consultant for biotech companies and investment firms. He is cofounder and CEO for EidoSearch, an Ontario based company offering a content-based search and analysis engine for financial big data.

Dr. Zhang is a registered Professional Engineer in Ontario, Canada, and a member of Beta Gamma Sigma Honor Society. He is the general co-chair for ICASSP2021. He is the general co-chair for 2017 GlobalSIP Symposium on Signal and Information Processing for Finance and Business. He is an elected member of ICME steering committee. He is the general chair for MMSP'15. He is the publicity chair for ICME'06 and program chair for ICLC'05 and ICIC'10. He served as guest editor for Multimedia Tools and Applications, and the International Journal of Semantic Computing. He is a tutorial speaker in ACMMM2011, ISCAS2013, ICIP2013, ICASSP2014, IJCNN2017. He is a Senior Area Editor for IEEE Transactions on Signal Processing. He is/was an Associate Editor for IEEE Transactions on Image Processing, IEEE Transactions on Multimedia, IEEE Transactions on Circuits and Systems for Video Technology, IEEE Transactions on Signal Processing, IEEE Signal Processing Letters and for Journal of Multimedia.